Enhancing Voltage Stability under GCC Constraints with the AI-Driven Optimization of Distributed Generators

Nasyith Hananur Rohiem
Electrical Engineering Department, Institut Teknologi Sepuluh Nopember, Surabaya, Indonesia
7022201014@student.its.ac.id

Adi Soeprijanto
Electrical Engineering Department, Institut Teknologi Sepuluh Nopember, Surabaya, Indonesia
adisup@its.ac.id (corresponding author)

Mat Syai'in
Department of Marine Electrical Engineering, Surabaya Shipbuilding State, Indonesia
matt.syaiin@ppns.ac.id

Received: 3 June 2025 | Revised: 12 August 2025 | Accepted: 20 August 2025

 DOI: https://doi.org/10.48084/etasr.12532

ABSTRACT

This paper presents a novel, data-driven, multi-objective optimization framework that uses Grasshopper Optimization Algorithm (GOA), Adaptive GOA (AGOA), and Flower Pollination Algorithm (FPA) to manage the active and reactive power outputs of Distributed Generators (DGs) within the limits of the AI-modeled Generator Capability Curve (GCC). This improves the voltage profiles and reduces the voltage unbalance in the distribution systems. The proposed method entails two steps. First, the GCC is reconstructed using a Deep Learning (DL) model with 20 neurons and 16 hidden layers. This model is trained utilizing numerical data for 2.5 MW and 3.0 MW DGs and achieves a minimum Mean Squared Error (MSE) of 1×10^{-8}. Second, the reconstructed GCC is integrated as a dynamic constraint in the optimization model to guide the DG dispatch. Three metaheuristic algorithms were applied to optimize the DG operation under unbalanced loading conditions at buses 10 and 15. AGOA had the best performance, reducing the voltage unbalance from 2.2129% to 1.4086% at bus 10 and from 2.0820% to 1.4295% at bus 15. AGOA also restored the voltage at bus 15 from 0.8698 p.u. to over 0.926 p.u. and achieved the lowest convergence fitness (<1.43). These results confirm AGOA's effectiveness in enhancing the voltage stability and phase balance, emphasizing the advantages of integrating DL-based GCC modeling with adaptive metaheuristic optimization for reliable and efficient DG operation.

Keywords-improving voltage profiles; reducing voltage unbalance; deep learning; GCC; metaheuristic algorithms

I. INTRODUCTION

Voltage unbalance is a persistent challenge in distribution networks, especially with the increasing integration of Distributed Generation (DG) sources [1, 2]. This can lead to reduced voltage levels, which can jeopardize the network safety, stability, and reliability. While the integration of the DG units can enhance the voltage profiles [3-5], and reduce the unbalance levels [1, 6], the variability of the DG output requires careful regulation. One effective approach is to operate DG units within the limits defined by the GCC, which prescribessafe operational boundaries for active and reactive power [7-10]. Operating within these limits improves safety and allows for higher power injection than static limits (P_{min}, P_{max}, Q_{min}, and Q_{max}) [11-13]. This reduces risks, such as thermal overload and instability. Implementing analytically derived GCCs in real-world systems remains challenging because the dynamic and nonlinear behavior of the power systems under unbalanced loading often reduces their accuracy [9, 10, 14]. Artificial intelligence (AI)-based reconstruction of GCCs has emerged as a promising alternative, capable of capturing the nonlinear patterns, adapting to different operating conditions, and improving the predictive accuracy [7, 8]. This permits more precise DG operation within the GCC limits, especially under unbalanced scenarios. Advanced metaheuristic algorithms have been applied to optimize the DG performance within AI-reconstructed GCC boundaries [4, 15-17]. GOA balances the exploration and exploitation [15, 18], AGOA [16] improves the accuracy through adaptive control, and FPA [17,

19] efficiently handles multi-objective optimization with minimal parameter tuning. These algorithms offer strong global search ability, fast convergence, and ease of application. However, existing methods often underperform under severe and persistent unbalanced load conditions. This study proposes a novel, multi-objective optimization framework combining GOA, AGOA, and FPA to manage the DG active and reactive power outputs within AI-modeled GCC limits. The framework aims to reduce the voltage unbalance below the IEEE 2% threshold, improve the voltage profile stability, and enhance the operational safety, contributing to the development of adaptive and resilient power distribution systems under high DG penetration.

II. THEORETICAL BACKGROUND AND RECONSTRUCTION OF THE GENERATOR CAPABILITY CURVE

The GCC determines the safe operating region for a synchronous generator in the *P*-*Q* plane, balancing the active power (*P*) and reactive power (*Q*) output under constraints. The modeling used in this study adheres to the standard formulation and physical constraints [20, 21], thereby ensuring the accurate design of the curve. The following three primary limits must be considered: The capability is defined by the Synchronous Stability Limit (SSL), the armature current limit, and the field current limit, which ensure stable, thermally safe operation within permissible excitation levels.

A. Theoretical Background

1) Synchronous Stability Limit

SSL represents the maximum *P* that can be delivered at a given *Q*, ensuring that the generator maintains synchronism. This limit is derived from the power-angle relationship of synchronous machines, with the power angle δ constrained to a maximum value δ_{max} to maintain stability, as shown in (4). The relationship between the stability limit and the *P* and *Q* power parameters of a synchronous generator is:

$$P = \frac{EV}{X_s} sin\ \delta \quad (1)$$

$$Q = \frac{V}{X_s}(\mathrm{E}\cos\delta - V) \quad (2)$$

where *P* is the active power delivered by the generator, *E* is the internal EMF, *V* is the terminal voltage, X_s is the synchronous reactance, and δ is the power angle. In order to enforce synchronism, δ is restricted to δ_{max}, which is typically set below 90°. Substituting $\delta=\delta_{max}$ and solving for *P* allows for the expression of E in terms of the known quantities *V*, *Q*, and X_s, and then *E* is inserted into:

$$E = \frac{QX_s+V^2}{V\ cos\ \delta_{max}} \quad (3)$$

$$P = \left(Q + \frac{V^2}{X_s}\right)\tan\delta_{max} \quad (4)$$

2) Armature Current Limit

The apparent power S, which integrates active and reactive power, is a crucial parameter in the GCC:

$$S = VI = \sqrt{P^2 + Q^2} \quad (5)$$

If the maximum armature current I_{max} is specified, then the apparent power limit is:

$$S \le VI_{max} \quad (6)$$

$$P^2 + Q^2 \le VI_{max} \quad (7)$$

With this, a circular boundary in the *P*-*Q* plane is defined, centered at the origin with radius $V.I_{max}$. The circle represents the maximum allowable combinations of *P* and *Q* that the generator can deliver without exceeding the armature current limit, thereby preventing overheating.

3) Field Current Limit

The field current limit is a crucial component in the overall design, as it functions to constrain the generator's internal Electromotive Force (EMF), E_a, which is proportional to the field current. This constraint is important to prevent the occurrence of overheating in the field winding, within a thermal and magnetic threshold $E_{a,max}$. Upon reaching this threshold, the generator operates at maximum excitation, thereby constraining the range of the feasible combinations of *P* and Q. The active power *P* is defined by the terminal voltage *V*, the internal EMF E_a, and the synchronous reactance X_s, as:

$$P = \frac{E_aV}{X_s} sin\ \delta \quad (8)$$

Q is the component of power that is 90o out of phase with *V*. Therefore, it can be expressed in terms of E_a, *V*, X_s, and the power angle, δ, which is the angle between E_a and *V*, as shown in Figure 1:

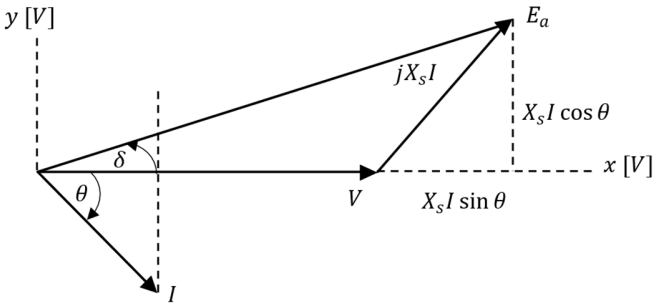

Fig. 1. Phasor plot diagram.

$$E_a = V + jX_sI \quad (9)$$

$$I = \frac{E_a - V}{jX_s} \quad (10)$$

$$Q = \frac{E_aV}{X_s}\cos\delta - \frac{V^2}{X_s} \quad (11)$$

where $\left(\frac{E_aV}{X_s}\cos\delta\right)$ is the reactive power contributed by the alignment of E_a and *V* and is influenced by the angle δ. This component shows that *Q* increases with both E_a and $\cos\delta$, and $\left(-\frac{V^2}{X_s}\right)$ is the reactive power needed to overcome the synchronous reactance X_s at no load (when $Q = 0$). This term acts as an offset, which accounts for the generator's inherent reactive power demand to sustain its internal voltage. The internal EMF of the synchronous generator E_a, is influenced by

the generator's terminal voltage V, the synchronous reactance X_s, the armature current I, and the power factor angle θ_{pf}:

$$E_a = \sqrt{\left(V + X_s I \sin\theta_{pf}\right)^2 + \left(X_s I \cos\theta_{pf}\right)^2} \quad (12)$$

B. Reconstruction of GCC

The GCC defines the parameters of feasible generator operation, thereby ensuring reliability and efficiency. However, its practical application is constrained by nonlinearities, the complexity of the computations, and the dynamic behavior of the grid. DL [22] presents a scalable, data-driven approach that captures complex relationships for real-time GCC approximation with reduced computational expense. The proposed framework capitalizes on these strengths to facilitate an efficient GCC reconstruction.

1) Data Preparation

Figure 2 (a) shows that the conversion of the dataset [7, 10] from the numerical outcomes of P and Q at x-y GCC coordinates is performed to yield θ, and R, respectively. To acknowledge the DG capacity, a unique code (n) is used as 1 for the first DG capacity and 2 for the second DG capacity:

$$R = \sqrt{P^2 + Q^2} \quad (13)$$

$$\theta = tan^{-1}\left(\frac{Q}{P}\right) \quad (14)$$

2) DL GCC Architecture

The DL GCC architecture consists of two inputs (n and θ) and a single output (R_{ref}), as depicted in Figure 2 (b).

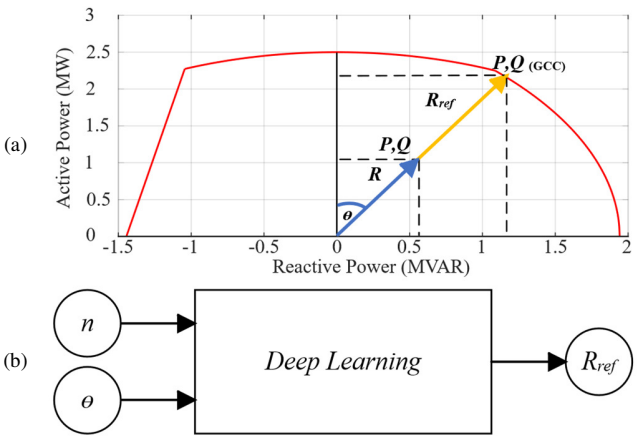

Fig. 2. (a) GCC data signals and (b) DL architecture.

3) Training Process

The network is trained using the Levenberg–Marquardt algorithm [23], with the neurons ranging from 5–20 and layers from 3–15. The data are partitioned by index, with 80% allocated for training and 20% for testing, in order to maintain the structural consistency. The performance of the model is evaluated using MSE [23], where lower values indicate better generalization and GCC reconstruction accuracy:

$$MSE = \frac{1}{n}\sum_{i=1}^{n}(a - p)^2 \quad (15)$$

where a is the actual value, p is the predicted value, and n is the number of samples.

4) DL GCC Implementation

Figure 3 portrays the DL GCC design system predicated on data preparation and the DL GCC architecture from Figure 2. The model functions by predicting the reference radius R_{ref}, which is subsequently compared to the actual radius R using:

$$R_{stat} = R_{ref} - R \quad (16)$$

A positive R_{stat} indicates operation within the DL GCC boundary, signifying safe conditions, while a negative value indicates operation beyond the DL GCC limit, highlighting potentially unsafe generator states. This predictive mechanism enables real-time monitoring and generator capability management.

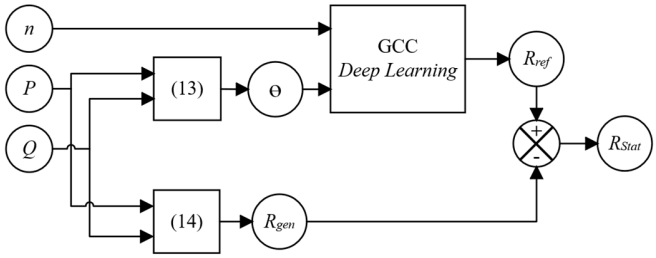

Fig. 3. DL GCC design system.

III. PROBLEM FORMULATION AND SYSTEM DESCRIPTION

Modern distribution systems are confronted with challenges, such as voltage imbalances and deficient voltage profiles, reducing efficiency, compromising stability, and accelerating equipment degradation. The usage of DG-based power injection with static capability limits [11-13] reduced the unbalance by 1.1%–1.5% while maintaining voltages within 0.95 p.u.–1.05 p.u. However, these fixed-boundary methods are not adaptable to dynamic grid conditions. The present study puts forth a novel proposal in the form of an AI-driven optimization framework. This framework has the capacity to reconstruct the GCC constraints, enabling the enhancement of adaptive voltage regulation and grid resilience.

A. Problem Formulation

In order to address issues, such as voltage unbalance, suboptimal profiles, and GCC constraints, a multi-objective optimization framework is proposed, maintaining voltage within safe limits, minimizing the phase deviations for stability, and regulating the DG output based on GCC. This integrated approach improves the grid resilience and optimizes the distribution performance.

1) Formulation of the Objective Functions

The optimization problem is expressed as a minimization of two key objective functions (1), (6), and each objective function addresses a specific aspect of the network performance:

$$f_{min} = w_1.U + w_2.V_{dev} \quad (17)$$

$$U = \frac{\sum_{i=n}^{n}|V_{a,i}-V_{b,i}|+|V_{b,i}-V_{c,i}|+|V_{c,i}-V_{a,i}|}{3n} \quad (18)$$

$$V_{dev} = \sum_{i=n}^{n} max\ (0, V_{min} - V_i) max\ (0, V_i - V_{max}) \quad (19)$$

where V_{min}, V_{max} are the minimum and maximum allowable voltage limits, respectively.

2) Constraints

In order to ensure that the operation is both feasible and stable, as well as safe, the optimization problem must satisfy several key constraints. These include limits related to the GCC, voltage imbalance, and voltage profile:

- GCC constraints: the safe operation for the GCC limits is described by:

$$R_{stats} = \begin{cases} < 0,\ unsafe \\ > 0,\ safe \end{cases} \quad (20)$$

- Voltage unbalance constraint: to maintain the network stability and prevent the equipment damage, the voltage unbalance should remain within a permissible limit as:

$$U \leq U_{max} \quad (21)$$

where U_{max} is the maximum allowable voltage unbalance index based on IEEE Std. 141-1999, and is set to 2%.

- Voltage profile constraints: the voltage at each node must be within a specified range to avoid the undervoltage or overvoltage conditions to ensuring system stability as [24]:

$$V_{min} \leq V_i \leq V_{max} \quad (22)$$

where V_{min}, V_{max} (range from 0.90 p.u to 1.05 p.u) are the minimum and maximum allowable voltages.

B. Benchmark System

The IEEE 15-bus system, equipped with DGs at buses 5, 8, 10, and 15, serves as the benchmark [25]. The capacity of the individual turbines is: DG1 (bus 15) and DG2 (bus 5), which are rated at 3 MW, while DG3 (bus 8) and DG4 (bus 10) are rated at 2.5 MW. The power flow is calculated using the ZBR-based load flow method [4, 26], enabling an accurate voltage estimation in radial networks. Notable voltage improvements have been observed at buses 15 and 10, enhancing the reliability, safety, and efficiency in the DG performance assessment.

C. Optimization Techniques

The power outputs (P, Q) of the DG are optimized using the following algorithms: the GOA [15, 16], the AGOA [16, 17], and the FPA [17, 19]. These algorithms ensure optimal performance and GOA achieves a balanced equilibrium between exploration and exploitation through the usage of grasshopper-inspired dynamics. The AGOA model incorporates adaptivity to enhance the accuracy and circumvent local optima. FPA uses Lévy flights to facilitate an efficient global search and precise local refinement. The integration of these two approaches enables the usage of each method's distinct strengths, thereby promoting the understanding of the efficacy of the optimization strategies.

D. Grasshopper Optimization Algorithm

GOA uses a hybrid approach that integrates elements of both exploration and exploitation to optimize solutions. The configuration of the grasshopper is subject to modification in accordance with the dynamics of mutual interactions and the degree of attraction to the prevailing optimal solution. The exploration-exploitation coefficient, C, and the position are updated according to [15, 16]:

$$C = C_{max} - j\left(\frac{C_{max}-C_{min}}{j_{max}}\right) \quad (23)$$

where C_{max}, C_{min} are constants, j, j_{max} are the current iteration and maximum iteration.

$$P_{(i)} = C\left(\sum_{\substack{j=1, \\ J\neq i}}^{N} s(d_{ij}).P_i - P_j\right) + P_{best} \quad (24)$$

where P_i, P_j are the grasshopper positions, $s(d_{ij})$ is the social interaction based on distance d_{ij}, and P_{best} is the current the best solution.

E. Adaptive Grasshopper Optimization Algorithm

AGOA enhances the standard GOA by introducing an adaptive coefficient into the position update [16]. It is important to note that this coefficient, A_j, undergoes dynamic adjustment with each iteration. In instances where A_j is less than 0.5, AGOA implements the Levy Flight Distribution (LFD) for exploratory analysis. In the absence of this condition, the system employs a spiral path update for exploitation [17]. This adaptive mechanism improves the convergence efficiency by effectively balancing the exploration and exploitation:

$$P_{(i)} = C\left(\sum_{\substack{j=1, \\ J\neq i}}^{N} s(d_{ij}).P_i - P_j\right) + A_j.P_{best} \quad (25)$$

$$A_j = A_{min} + j\left(\frac{A_{max}-A_{min}}{j_{max}}\right) \quad (26)$$

where A_{max}, A_{min} are the maximum and minimum adaptive values

$$P_{(i)} = P_{(i)} + Levy.(P_{(i)} - P_{best}) \quad (27)$$

$$P_{(i)} = \left|P_{best} - P_{(i)}\right|.e^{bj}.\cos 2\pi j + P_{best} \quad (28)$$

where b is a constant value.

F. Flower Pollination Algorithm

FPA replicates natural pollination processes, achieving an effective balance between the global and local searches [17, 19]. In the context of global search, the algorithm introduces novel search areas by leveraging LFD (Local Search Heuristic) [17]. The usage of alternating search strategies is important for ensuring the efficacy of exploration and exploitation, thereby enhancing the quality of the solutions and facilitating the optimal DG generation:

$$P_i^{t+1} = P_i^t + \gamma.L(\lambda).(P_g - P_i^t) \quad (29)$$

where P_i^t is the solution at iteration t, P_g is the global best solution, γ is a scaling factor, and $L(\lambda)$ is the LFD step size.

$$P_i^{t+1} = P_i^t + \epsilon.(P_j - P_k) \quad (30)$$

where P_j and P_k represent randomly selected solutions and ϵ is a random factor.

IV. RESULTS AND DISCUSSION

The simulation results in this paper were carried out based on the following steps:

A. GCC Construction Using a Numerical Approach

Figure 4 presents the GCCs for 2.5 MW and 3.0 MW generators that were developed through numerical modeling to delineate feasible *P-Q* operating regions under thermal and power factor constraints. Authors in [20] examined key parameters that were adapted to align with the practical and simulation needs of this study. The *P-Q* curve of the 3.0 MW unit serves as reference baseline for the subsequent data-driven reconstruction.

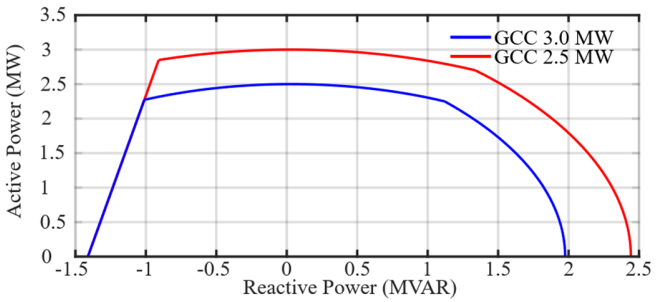

Fig. 4. GCC results with 2.5 MW capacity and 3.0 MW capacity.

B. Reconstruction of DL GCC

In order to maintain the integrity of the generator class, the dataset was appropriately indexed, with 80% allocated for training and 20% designated for testing, without the need for random shuffling. The DG code *n* denotes the generator type, with *n* = 1 indicating a 2.5 MW generator and *n* = 2 indicating a 3.0 MW generator. The original (*P*, *Q*) data were transformed into polar form. The optimization of the model was achieved through the use of a randomized search algorithm for the determination of neuron counts (5–20) and hidden layers (3–15), with the validation process being conducted using the MSE metric. As displayed in Table I, a number of configurations have been previously tested and compared, offering substantiation for the efficacy of the method in reconstructing the DL GCC. The optimal configuration, comprising 20 neurons and 16 layers, was identified through a systematic process of experimentation. This configuration was selected based on the lowest MSE value obtained from the model.

TABLE I. CONFIGURATION AND COMPARATIVE RESULTS

Neurons	Hidden Layers	MSE
6	12	0.00080900
7	7	0.00016000
14	13	0.00000002
20	16	0.00000001
18	14	0.00000002
12	8	0.00007200

C. Voltage Profile and Unbalance Analysis of the Benchmark System

The benchmark radial distribution system incorporates nominally balanced loads, with deliberate asymmetry at buses 10 and 15 to evaluate the system's sensitivity to unbalanced conditions. At bus 10, the active and reactive powers across phases are (0.21 MW, 0.24 MW, 0.27 MW) and (0.18 MVAR, 0.21 MVAR, 0.24 MVAR), respectively. Bus 15 shows (0.10 MW, 0.12 MW, 0.15 MW) and (0.18 MVAR, 0.15 MVAR, 0.12 MVAR). Figure 5 presents the voltage magnitudes, unbalance, and phase angles. Voltage fluctuations have been recorded at buses 10 and 15, with voltage imbalances reaching 2.21% and 2.08%, respectively. These values exceed the standard 2% threshold. The phase angles maintain the proximity to the ideal 1200, thereby substantiating the impact of moderate asymmetry on the voltage quality.

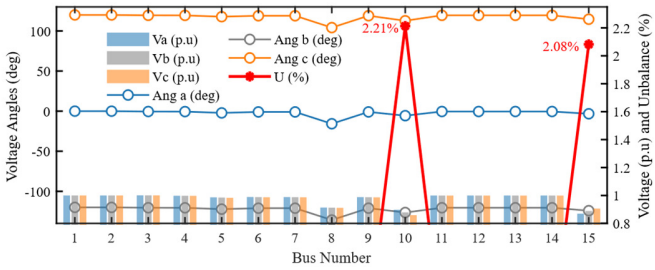

Fig. 5. Existing condition from benchmark system.

D. Analysis of DL GCC Implementation

The efficacy of the proposed DL-GCC design is confirmed through a comparison of the DG operating points with and without DL-based GCC enforcement. For the 2.5 MW unit, the model with GCC constraints maintains the majority of points within the defined capability boundary, as illustrated in Figure 6. In contrast, the unconstrained case exhibits frequent violations, indicating an increased risk of instability. The findings of this study substantiate the pivotal function of the DL-GCC module in facilitating secure dispatch by means of dynamically constraining the real and reactive power. The predictive margin R_{stat} supports the real-time supervisory control and proactive generator management.

E. Optimization DG Performance within DL GCC

In this context, the DG operation adhered to its GCC constraints with the objective of enhancing the bus voltage profiles and reducing the voltage unbalance. The DG operated within the defined limits of P_{min}, P_{max}, Q_{min}, and Q_{max}, as indicated by the actual capability curve, while the Optimal Power Injection (OPI) was determined using the GOA, the AGOA, and the FPA, each configured with a population of 25 and 100 iterations. The multi-objective function (17) allocates weights w_1=0.095 for the unbalance minimization and w_2=0.905 for the voltage profile enhancement, as presented in Table II. The optimal generation results for each DG, as shown in Figure 7, and algorithm were thoroughly evaluated with the DL GCC to ascertain the feasibility and operational safety. According to the findings, under the FPA, DG1 generated 0.60 MW / 0.59 MVAR, while DG4 produced 0.50 MW / 0.69

MVAR. Notably, DG2 and DG3 were observed to be in a state of inactivity. GOA exhibited a comparable trend, with DG1 at 0.60 MW / 0.59 MVAR and DG4 at 0.50 MW / 0.74 MVAR. Conversely, AGOA adopted a more distributed approach: DG1 contributed 0.53 MW / 0.59 MVAR, DG3 provided 0.26 MW / 1.28 MVAR, and DG4 generated 0.41 MW / 0.68 MVAR, while DG2 was not dispatched. It was determined that all operating points selected by the algorithms were within the bounds defined by the DL GCC. Furthermore, AGOA demonstrated an ability to use a wider portion of the feasible region. This distribution across multiple units enhanced the system's reactive power support and thermal usage, thereby reinforcing the local voltage and reducing the stress on any individual DG unit. Furthermore, each algorithm was capable of determining the optimal commitment status for each DG, hence indicating the necessary adjustments to allocate units in order to maintain equilibrium between the supply and demand, as well as to avert the network overloads.

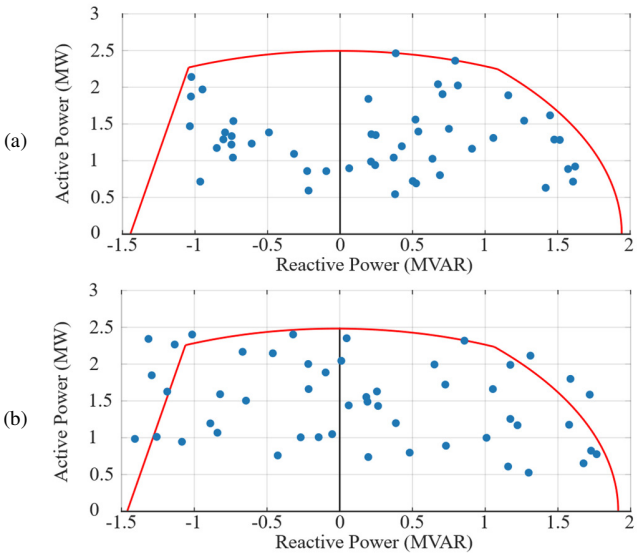

Fig. 6. DG operating point: (a) with and (b) without DL GCC limit.

TABLE II. ALGORITHM PARAMETERS SETTING

Parameters	GOA	AGOA	FPA
C_{min}	0.0001	0.0001	-
C_{max}	0.001	0.001	-
A_{min}	0.35	0.35	-
A_{max}	0.85	0.85	-
Switching probability (p)	-	-	0.8

The convergence behavior further confirmed AGOA's superiority: the convergence curve indicated that AGOA achieved the lowest final fitness value and reached stability earlier than GOA and FPA. This finding suggests that AGOA exhibits a superior equilibrium between exploration and exploitation in the optimization process, thereby yielding more robust and effective solutions, as portrayed in Figure 8. AGOA exhibited the lowest voltage unbalance across the 15-bus system, with a peak of 1.4295%, in comparison to 1.4459% (FPA) and 1.4462% (GOA). It is noteworthy that AGOA maintained the imbalance at bus 10 at 1.4086%, which is slightly superior to the FPA and GOA. The usage of DG3 under AGOA introduced novel injection points and contributed substantially to the phase balance, thereby reinforcing the weak segments of the distribution network.

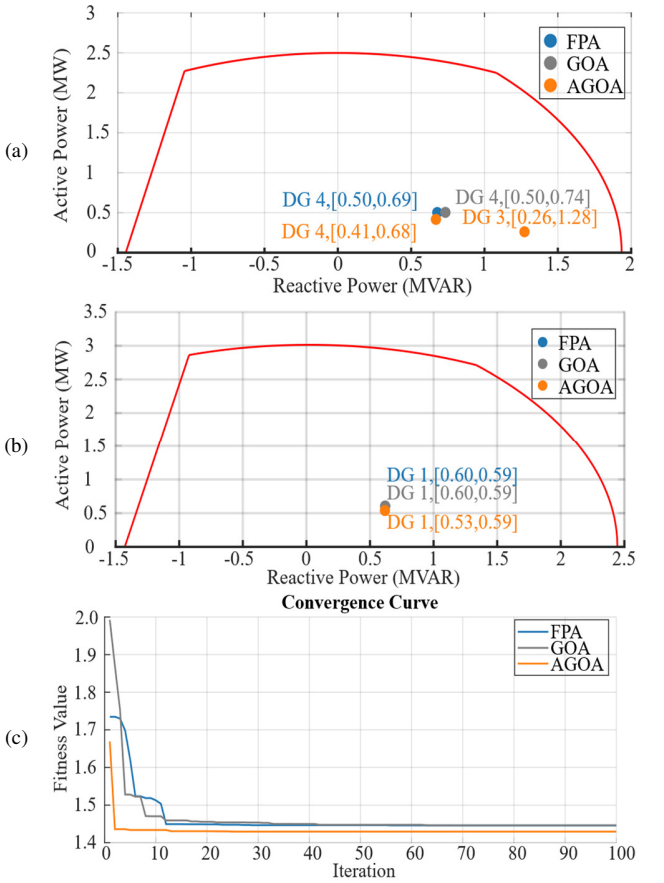

Fig. 7. Optimization results: (a) 2.5 MW DG GCC, (b) 3.0 MW DG GCC, and (c) convergence curve.

The voltage magnitude and angle results shown in Figures 8 (a-c) demonstrate significant enhancements at buses 10 and 15, which exhibited the least substantial base voltages. Subsequent to optimization, bus 15 increased from 0.8698 p.u. to above 0.92 p.u., and bus 10 also gained voltage support. The three algorithms (FPA, GOA, AGOA) exhibited consistent voltage levels within the range of 22, while the angles remained close to 120°, with AGOA yielding the most stable outcomes, particularly at buses 8–10. A comparison with the existing condition reveals the clear benefits of optimization, exhibiting voltage unbalance violations at bus 10 (2.2129%) and bus 15 (2.0820%), which exceeded the acceptable 2% limit. Furthermore, a dangerously low voltage magnitude of 0.8698 p.u. was observed at bus 15. Conversely, AGOA and the other algorithms maintained all bus voltages above 0.92 p.u. and eliminated the unbalance violations entirely. The findings indicate that the integration of GCC-aware optimization strategies, particularly those leveraging AGOA, results in a substantial enhancement of the power quality, operating margin, and system robustness within real-world distribution networks.

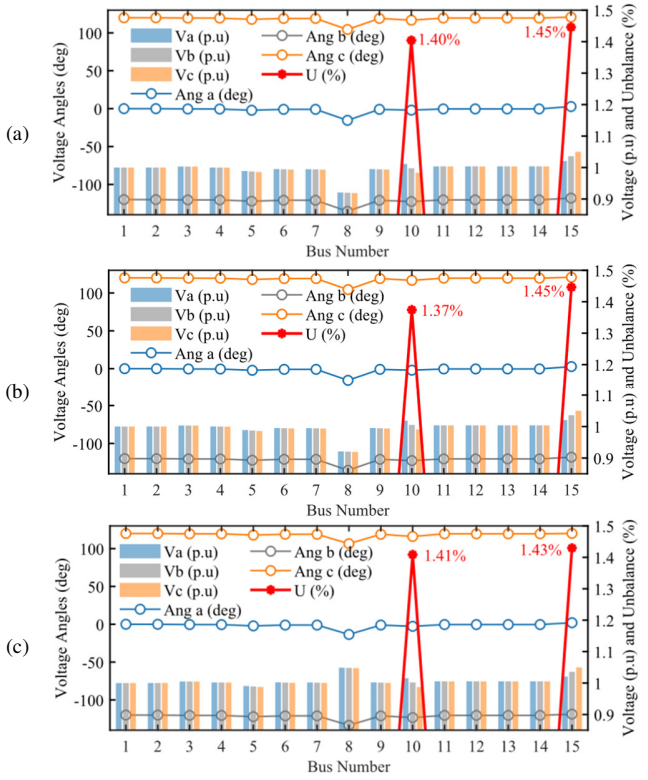

Fig. 8. Voltage profile and unbalance percentage condition after optimization using: (a) FPA, (b) GOA, and (c) AGOA.

V. CONCLUSIONS

The present study examines the hypothesis that the integration of DL Generator Capability Curve (GCC) modeling with metaheuristic optimization significantly enhances the voltage regulation and reduces the unbalance in distribution systems. The Deep Learning (DL) model was able to accurately reconstruct the boundaries of GCC for 2.5 MW and 3.0 MW DG units, achieving a minimum Mean Squared Error (MSE) of 1×10-8 using a configuration of 20 neurons and 16 hidden layers. It is evident that all optimization methods, Flower Pollination Algorithm (FPA), Grasshopper Optimization Algorithm (GOA), and Adaptive GOA (AGOA), effectively operated Distributed Generators (DGs) within safe GCC limits while achieving the performance objectives. Among the aforementioned, AGOA yielded the most favorable outcomes, with a reduction in the voltage unbalance at bus 10 from 2.2129% to 1.4086% and at bus 15 from 2.0820% to 1.4295%. Additionally, it restored voltage at bus 15 from a critical 0.8698 p.u. in the existing condition to above 0.926 p.u., thus ensuring that all bus voltages remained within the acceptable range. With respect to the distribution of power, AGOA optimally dispatched DG1 at 0.53 MW / 0.59 MVAR, DG3 at 0.26 MW / 1.28 MVAR, and DG4 at 0.41 MW / 0.68 MVAR. This configuration resulted in enhanced voltage support and reduced the thermal stress across units. The convergence analysis further substantiated the efficacy of AGOA, with a final fitness value below 1.43, surpassing FPA and GOA in terms of both the accuracy and processing speed. Furthermore, the algorithms dynamically allocate or deallocate the DG units to maintain equilibrium between the active and reactive power supply without inducing network overload. These findings affirm that DL GCC-constrained, AI-assisted optimization is a practical and robust approach for achieving high-quality voltage profiles and minimizing the unbalance in distribution grid operations.

ACKNOWLEDGMENT

This work was supported by the Indonesia Endowment Funds for Education (LPDP) Center for Center for Higher Education Funding and Assessment (PPAPT) Ministry of Higher Education, Science, and Technology of the Republic of Indonesia.

REFERENCES

[1] A. S. Vijay, S. Doolla, and M. C. Chandorkar, "Unbalance mitigation strategies in microgrids," *IET Power Electronics*, vol. 13, no. 9, pp. 1687–1710, 2020, https://doi.org/10.1049/iet-pel.2019.1080.

[2] S. A. Taher and M. H. Karimi, "Optimal reconfiguration and DG allocation in balanced and unbalanced distribution systems," *Ain Shams Engineering Journal*, vol. 5, no. 3, pp. 735–749, Sept. 2014, https://doi.org/10.1016/j.asej.2014.03.009.

[3] M. R. Haddad and M. Y. Al-Suliman, "Voltage Profile Improvement Based on Optimal Allocation and Sizing Distributed Generation," in *2024 21st International Multi-Conference on Systems, Signals & Devices (SSD)*, Erbil, Iraq, Apr. 2024, pp. 239–244, https://doi.org/10.1109/SSD61670.2024.10548836.

[4] N. H. Rohiem, A. Soeprijanto, and M. Syai'in, "Optimal Placement and Sizing of Multiple DGs in an Unbalanced Load Flow Using GOA Direct-ZBR and AGOA Direct-ZBR Methods to Determine The Lowest Active Power Loss Value," in *2023 International Conference on Advanced Mechatronics, Intelligent Manufacture and Industrial Automation, ICAMIMIA 2023*, Lombok, Indonesia, 2023, pp. 324–329, https://doi.org/10.1109/ICAMIMIA60881.2023.10427715.

[5] M. Salman, S. Hongsheng, M. A. Aman, and Y. Khan, "Enhancing Voltage Profile and Power Loss Reduction Considering Distributed Generation (DG) Resources," *Engineering, Technology & Applied Science Research*, vol. 12, no. 4, pp. 8864–8871, Aug. 2022, https://doi.org/10.48084/etasr.5046.

[6] H. Çimen and N. Çetinkaya, "Voltage sensitivity-based demand-side management to reduce voltage unbalance in islanded microgrids," *IET Renewable Power Generation*, vol. 13, no. 13, pp. 2367–2375, 2019, https://doi.org/10.1049/iet-rpg.2018.5603.

[7] C.-Y. Lee and M. Tuegeh, "Virtual Visualization of Generator Operation Condition through Generator Capability Curve," *Energies*, vol. 14, no. 1, Jan. 2021, Art. no. 185, https://doi.org/10.3390/en14010185.

[8] M. Syai'in, K. L. Lian, and A. Soeprijanto, "Digital Generator Capability Curve for Improving Optimal Power Flow based on IPSO," *International Review of Electrical Engineering (IREE)*, vol. 8, no. 2, pp. 912–919, Apr. 2013, https://doi.org/10.15866/iree.v8i2.1794.

[9] A. Flores, R. Zárate-Miñano, and M. Carrión, "Capability Curve Modeling for Hydro-Power Generators in Optimal Power Flow Problems," *Sustainability*, vol. 15, no. 24, Jan. 2023, Art. no. 16654, https://doi.org/10.3390/su152416654.

[10] M. Syai'in, A. Soeprijanto, I. M. Y. Negara, and M. Mahfud, "Incremental Particle Swarm Optimizer with local search for Optimal Power Flow Subjected to Digital GCC based on Neural Network," *International Journal of Digital Content Technology and its Applications*, vol. 6, no. 7, pp. 242–252, 2012.

[11] F. C. R. Coelho, W. Peres, Ivo. C. Silva Júnior, and B. H. Dias, "Empirical continuous metaheuristic for multiple distributed generation scheduling considering energy loss minimisation, voltage and unbalance regulatory limits," *IET Generation, Transmission & Distribution*, vol. 14, no. 16, pp. 3301–3309, 2020, https://doi.org/10.1049/iet-gtd.2019.1860.

[12] M. Kazeminejad, M. Banejad, U. D. Annakkage, and N. Hosseinzadeh, "Load pattern-based voltage stability analysis in unbalanced distribution networks considering maximum penetration level of distributed generation," *IET Renewable Power Generation*, vol. 14, no. 13, pp. 2517–2525, 2020, https://doi.org/10.1049/iet-rpg.2019.1196.

[13] E. S. Ali, R. A. El-Sehiemy, A. A. A. El-Ela, S. Kamel, and B. Khan, "Optimal planning of uncertain renewable energy sources in unbalanced distribution systems by a multi-objective hybrid PSO–SCO algorithm," *IET Renewable Power Generation*, vol. 16, no. 10, pp. 2111–2124, 2022, https://doi.org/10.1049/rpg2.12499.

[14] *Reliability Guideline: Power Plant Model Verification for Inverter-Based Resources*. Atlanta, GA,, USA: NERC, 2018.

[15] S. Saremi, S. Mirjalili, S. Mirjalili, and J. Song Dong, "Grasshopper Optimization Algorithm: Theory, Literature Review, and Application in Hand Posture Estimation," in *Nature-Inspired Optimizers: Theories, Literature Reviews and Applications*, S. Mirjalili, J. Song Dong, and A. Lewis, Eds. Cham, Switzerland: Springer International Publishing, 2020, pp. 107–122.

[16] A. Alhejji, M. Ebeed Hussein, S. Kamel, and S. Alyami, "Optimal Power Flow Solution With an Embedded Center-Node Unified Power Flow Controller Using an Adaptive Grasshopper Optimization Algorithm," *IEEE Access*, vol. 8, pp. 119020–119037, 2020, https://doi.org/10.1109/ACCESS.2020.2993762.

[17] X.-S. Yang, *Nature-Inspired Optimization Algorithms*, 1st ed. London, UK: Elsevier, 2014.

[18] Y. Meraihi, A. B. Gabis, S. Mirjalili, and A. Ramdane-Cherif, "Grasshopper Optimization Algorithm: Theory, Variants, and Applications," *IEEE Access*, vol. 9, pp. 50001–50024, 2021, https://doi.org/10.1109/ACCESS.2021.3067597.

[19] S. Dhivya and R. Arul, "Improved Flower Pollination Algorithm-based Optimal Placement and Sizing of DG for Practical Indian 52 Bus System," in *2021 IEEE International IOT, Electronics and Mechatronics Conference (IEMTRONICS)*, Toronto, ON, Canada, Apr. 2021, pp. 1–5, https://doi.org/10.1109/IEMTRONICS52119.2021.9422562.

[20] S. J. Chapman, *Electric Machinery Fundamentals*, 5th ed. Melbourne, Australia: McGraw-Hill, 2012.

[21] J. Grainger, *Power system analysis*, 1st ed. Singapore: McGraw Hill, 1999.

[22] Y. LeCun, Y. Bengio, and G. Hinton, "Deep learning," *Nature*, vol. 521, no. 7553, pp. 436–444, May 2015, https://doi.org/10.1038/nature14539.

[23] S. Ali, S. Riaz, Safoora, X. Liu, and G. Wang, "A Levenberg–Marquardt Based Neural Network for Short-Term Load Forecasting," *Computers, Materials & Continua*, vol. 75, no. 1, pp. 1783–1800, 2023, https://doi.org/10.32604/cmc.2023.035736.

[24] *72:1987 - Standar Tegangan untuk Jaringan Tegangan Rendah*. Jakarta, Indonesia: Perusahaan Umum Listrik Negara (PLN), 1987.

[25] N. H. Rohiem, A. Soeprijanto, and M. Syai'in, "Multi-Objective Optimization for DG Placement and Sizing in Unbalanced Distribution Networks," in *2024 7th International Seminar on Research of Information Technology and Intelligent Systems (ISRITI)*, Yogyakarta, Indonesia, Sept. 2024, pp. 217–222, https://doi.org/10.1109/ISRITI64779.2024.10963504.

[26] T.-H. Chen and N.-C. Yang, "Three-phase power-flow by direct ZBR method for unbalanced radial distribution systems," *IET Generation, Transmission & Distribution*, vol. 3, no. 10, pp. 903–910, Oct. 2009, https://doi.org/10.1049/iet-gtd.2008.0616.